Synergistic effects of light-emitting probes and peptides for targeting and monitoring integrin expression

Samuel Achilefu*[†], Sharon Bloch*, Mary A. Markiewicz[‡], Tuoxiu Zhong[§], Yunpeng Ye*, Richard B. Dorshow*, Britton Chance[†§], and Kexian Liang*

Departments of *Radiology and [‡]Pathology and Immunology, Washington University School of Medicine, St. Louis, MO 63110; and [§]Department of Biochemistry and Biophysics, University of Pennsylvania, Philadelphia, PA 19104

Integrins mediate many biological processes, including tumor-induced angiogenesis and metastasis. The arginine–glycine–aspartic acid (RGD) peptide sequence is a common recognition motif by integrins in many proteins and small peptides. While evaluating a small library of RGD peptides for imaging $\alpha_v\beta_3$ integrin (ABI)-positive tumor cell line (A549) by optical methods, we discovered that conjugating a presumably inactive linear hexapeptide GRDSPK with a near-infrared carbocyanine molecular probe (Cypate) yielded a previously undescribed bioactive ligand (Cyp-GRD) that targets ABI-positive tumors. MTT [3-(4,5-dimethylthiazol-2-yl)-2,5-diphenyltetrazolium bromide] assay with A549 cells showed that Cyp-GRD was not cytotoxic up to 100 μM in cell culture. The compound was internalized by cells, and this internalization was blocked by coincubation with a cyclic RGD peptide (cyclo[RGDfV], f is D-phenylalanine) that binds ABI with high affinity. In vivo, Cyp-GRD selectively accumulated in tumors relative to surrounding normal tissues. Blocking studies with cyclo[RGDfV] inhibited the in vivo uptake of Cyp-GRD, suggesting that both compounds target the same active site of the protein. A strong correlation between the Cyp-GRD peptide and mitochondrial NADH concentration suggests that the new molecule could also report on the metabolic status of cells ex vivo. Interestingly, neither a Cypate-labeled linear RGD peptide nor an ^{111}In-labeled DOTA-GRD conjugate was selectively retained in the tumor. These results clearly demonstrate the synergistic effects of Cypate and GRD peptide for molecular recognition of integrin expression and suggest the potential of using carbocyanines as optical scaffolds for designing biologically active molecules.

mouse | optical imaging | RGD peptides | tumor | near-infrared

Angiogenesis, the formation of new blood vessels, is the cardinal feature of virtually all malignant tumors (1). Because of this commonality, probing tumor-induced angiogenesis and associated proteins is a viable approach to detect and treat a wide range of cancers. Angiogenesis is stimulated by integrins, a large family of transmembrane proteins that mediate dynamic linkages between extracellular adhesion molecules and the intracellular actin skeleton. Integrins are composed of two different subunits, α and β, which are noncovalently bound into $\alpha\beta$ complexes (2–4). Particularly, the expression of $\alpha_v\beta_3$ integrin (ABI) in tumor cells undergoing angiogenesis and on the epithelium of tumor-induced neovasculature alters the interaction of cells with the extracellular matrix, thereby increasing tumorigenicity and invasiveness of cancers (5–9).

Numerous studies have shown that ABI and more than seven other heterodimeric integrins recognize proteins and low molecular weight ligands containing RGD (arginine–glycine–aspartic acid) motifs in proteins and small peptides (10). Based on structural and bioactivity considerations, cyclic RGD peptide ligands are preferentially used as delivery vehicles for molecular probes for imaging (8, 11–13) and treating (14–17) ABI-positive tumors and proliferating blood vessels. Until recently, most of the in vivo imaging studies were performed with radiopharmaceuticals because of the high sensitivity and clinical utility of nuclear imaging methods. Particularly, the use of small monoatomic radioisotopes does not generally interfere with the biodistribution and bioactivity of ligands. Despite these advantages, nuclear imaging is currently only performed in specialized centers because of regulatory, production, and handling issues associated with radiopharmaceuticals. Optical imaging is an alternative but complementary method to interrogate molecular processes in vivo and in vitro.

Optical imaging for biomedical applications typically relies on activating chromophore systems with low energy radiation between 400 -and 1,500-nm wavelengths and monitoring the propagation of light in deep tissues with a charge-coupled device camera or other point source detectors (18). Molecular optical imaging of diseases with molecular probes is attractive because of the flexibility of altering the detectable spectral properties of the probes, especially in the fluorescence detection mode. The probes can be designed to target cellular and molecular processes at functional physiological concentrations. For deep-tissue imaging, molecular probes that are photoactive in the near-infrared (NIR) instead of visible wavelengths are preferred to minimize background tissue autofluorescence and light attenuation caused by absorption by intrinsic chromophores (19). In contrast to radioisotopes, the NIR antennas are usually large heteroatomic molecules that could impact the biodistribution and activity of conjugated bioactive ligands. However, previous studies have shown that conjugating small peptide carriers with NIR molecular probes successfully delivered the probes to target proteins in vivo, and the nonspecific distribution of the conjugate in nontarget tissues can be minimized by adjusting its net lipophilicity and ionic character (20).

We report herein a previously undescribed integrin-specific ligand prepared from two motifs that lack ABI recognizable motifs. One motif is a NIR carbocyanine fluorescent probe (Cypate) that is currently used to develop bioactive optical contrast agents (21), and the other is a linear hexapeptide (GRDSPK, abbreviated GRD) derived from the ABI-avid heptapeptide GRGDSPK (22) but lacking the RGD sequence. Intuitively, deletion of glycine in the linear RGD heptapeptide would be expected to diminish or eradicate the binding of the resulting GRD peptide to ABI because of alteration in the interatomic distances between the arginine and aspartic acid binding groups. Expectedly, the GRD peptide and its radiometal chelate conjugate (for scintigraphy) were not retained in the ABI-positive A549 tumor. In contrast, the Cypate-GRD conju-

---

gate (Cyp-GRD) was internalized in A549 cells *in vitro* and its uptake was inhibited by high affinity ABI-binding ligands. Particularly, antibody blocking studies demonstrates the effective inhibition of Cyp-GRD uptake by anti-β_3 monoclonal antibody (mAb) and to a lesser extent by anti-α_v mAb. This finding suggests that the β_3 subunit in ABI initiates the cellular uptake of Cyp-GRD by A549 cells. *In vivo*, the molecular probe preferentially accumulated in A549 tumors in nude mice. Co-administration of the probe with a high-affinity ABI-binding ligand successfully blocked the probe's uptake in the tumor, thereby demonstrating the specificity of the observed tumor retention of Cyp-GRD. These results demonstrate the synergistic effects of the tandem carbocyanine molecular probe and the peptide motif in targeting integrin-positive tumors. The findings suggest that the structural framework of the probe can serve as an optical scaffold to develop novel bioactive molecules for imaging diseases and potentially monitoring the efficacy of new drugs.

Materials and Methods

General. A detailed description of experimental methods is available in supporting information, which is published on the PNAS web site. All reagents and solvents were obtained from commercial sources and used without further purification. ABI-binding cyclo[GRGDfV], was purchased from Peptide International (Louisville, KY) and used for blocking studies. Oct-reotate, an octapeptide that binds somatostatin receptors but not ABI, was prepared as described (23). Purification and analysis of the new peptides were performed on an HPLC system equipped with a tunable UV-visible detector. Analytical (flow rate, 0.5 ml/min) and semipreparative (flow rate, 10 ml/min) reverse phase-HPLC were performed on C-18 columns using gradient elution and detected at 214 and 254 nm.

Synthesis of NIR Fluorescent Molecular Probe (Cypate). Cypate was prepared as described (24) starting with a functionalized quaternary benzoindole and glutaconaldehyde dianil mono hydrochloride to afford the desired compound in good yield.

Peptide Synthesis and Conjugation with Cypate and DOTA. The linear peptides were prepared by standard fluorenylmethyl (Fmoc) protocol (25), as described (21, 23). Conjugation of Cypate with peptides was performed on solid support. The cyclic peptide was prepared in three steps consisting of solid phase peptide synthesis, intramolecular lactamization in solution, and dye conjugation. Orthogonally protected tri-*tert*-butyl N',N'',N''',N''''-dodecyltetraacetic acid (tri-*t*-Bu DOTA) was coupled to the peptide on solid support, and the metal chelating DOTA-peptide conjugate was obtained by using the method described in ref. 26. The following compounds were prepared for this study: (*i*) Gly-Arg-Asp-Ser-Pro-Lys-OH (GRD), (*ii*) Cypate-Gly-Arg-Asp-Ser-Pro-Lys-OH (Cyp-GRD), (*iii*) Cypate-Gly-Arg-Gly-Asp-Ser-Pro-Lys-OH (Cyp-RGD), (*iv*) Cypate-cyclo[Arg-Gly-Asp-D-Phe-Val-Lys(ε-Cypate)] (Cyp-cyclo-RGD), and (*v*) DOTA-Gly-Arg-Asp-Ser-Pro-Lys-OH (DOTA-GRD).

Absorption and Emission Properties. The spectral properties of Cypate and their peptide conjugates were determined in 20% aqueous DMSO, using Beckman Coulter DU 640 spectrophotometer for absorption and Fluorolog-3 fluorometer for fluorescence measurements (see supporting information for details).

Fluorescence Microscopy and Internalization Studies. Cells were grown on LabTek microscope slides as described above. The medium was removed, and the cells were incubated at 4°C or 37°C in PBS containing 1 μM Cypate-RGD peptide or cypate dye alone for 30 min. For competition studies, the cells were preincubated with 1 μM unlabeled cyclo[RGDfV] for 15 min

before the addition of 1 μM Cyp-GRD. The cells were further incubated at 37°C for 30 min. For antibody blocking studies, cells were preincubated for 30 min at room temperature with 10 μg/ml function-specific monoclonal antibodies anti-α_v or anti-β_3 integrin subunits (Molecular Probes) before addition of 1 μM cypate-RGD peptide. For nuclear staining, 0.1 μM TOPO-1 (Molecular Probes) was mixed with mounting medium and applied to the cells incubated with Cyp-GRD. All cells were visualized on an Olympus FV1000 microscope equipped with the appropriate band width filters for Cyp-GRD (780 nm excitation, 830 emission) and TROPO-1 (470 excitation, 528 emission).

Cytotoxicity 3-(4,5-Dimethylthiazol-2-yl)-2,5-Diphenyltetrazolium Bromide (MTT) Assay. Cytotoxicity assays were performed by using the MTT *in vitro* toxicology assay kit from Sigma. The cell viability was calculated by taking the difference of the absorbances at 570 nm and 690 nm before and after the addition of MTT. Additional information is contained in the supporting information.

Whole-Body Small Animal Imaging by Reflectance Planar Fluorescence Imaging. All *in vivo* studies were performed in compliance with the Washington University Animal Study Committee's requirements for the care and use of laboratory animals in research. Nude mice (18–22 g) bearing 3- to 5-mm (diameter) tumors were anesthetized with xylazine/ketamine mixture before imaging. A noninvasive *in vivo* continuous wave fluorescence imaging apparatus was used to visualize the distribution and preferential tissue uptake of the Cyp-GRD in nude mice (20). The molecular probe (100 μl) was injected via the lateral tail vein at 0.3 μmol per kg of body weight. Details are given in supporting information.

***In Vivo* Competitive Blocking Studies.** The mice for competitive blocking studies were handled as described above. Equimolar amounts of the Cyp-GRD peptide conjugate and ABI-mediated angiogenesis inhibitor cyclo[Arg-Gly-Asp-D-Phe-Val] were constituted in a vial, and doses of 0.3 μmol/kg body weight were injected into the A549 tumor-bearing mice. Fluorescence images of the probe distribution in mice were monitored as a function of time. Data analysis was performed as described in the supporting information.

High-Resolution 3D Tumor Tissue Imaging with a Low-Temperature Fluorometric Redox Scanner. High-resolution spatial distribution of Cyp-GRD and the mitochondrial markers of cellular metabolic activity (NADH and flavoprotein, FP) was obtained by a snap-freeze method, as described (27). The frozen tumor sample was imaged in the Z direction by chipping the tumor tissue at 100-μm intervals. The fluorescence of FP, NADH, and Cyp-GRD were recorded digitally on a PC and reconstructed with MATLAB software. The redox ratio of NADH/(FP+NADH) calculated with MATLAB represented the reduced state of the mitochondria.

Results and Discussion

Molecular Design and Synthesis. Compounds containing the RGD peptide sequence are currently used as either antiangiogenic drugs (14–17) or carriers for radioisotopes (8, 12, 13) to target a variety of integrins. The improved binding affinity of cyclic peptides to integrins has inspired numerous research efforts toward their use in biomedical research (28–30). The glycine between arginine and aspartic acid in RGD provides a flexible orientation for molecular recognition of the arginine and aspartic acid residues by dimeric $\alpha\beta$ integrin subunits. This finding suggests that Arg and Asp constitute the active motif in most RGD molecular recognitions. Particularly, x-ray spectroscopy of the extracellular component of ABI crystals with (31) and without (32) a ligand shows that arginine and aspartic acid units
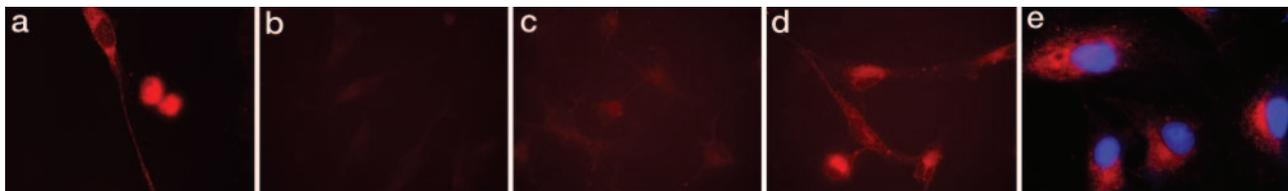
Fig. 1. Cellular uptake of molecular probes. (*a*) Internalization of Cyp-GRD in A549 cells incubated in 1 μM probe for 30 min at 37°C. (*b*) Inhibition of Cyp-GRD uptake by coincubation with 10 μM cyclo[GRDfV] and 1 μM Cyp-GRD at 37°C for 30 min. (*c*) Inhibition of Cyp-GRD uptake by coincubation with 10 μg/ml anti-β_3 monoclonal antibody and 1 μM of Cyp-RGD at 37°C for 30 min. (*d*) Low-level inhibition of Cyp-GRD uptake by coincubation with 10 μg/ml anti-α_v monoclonal antibody and 1 μM Cyp-RGD at 37°C for 30 min. (*e*) Cyp-GRD (red) and TROPO-1 (blue, nuclear stain) showing that probe is not localized in the nucleus. Images in *b*–*d* were normalized to the highest fluorescence intensity from *a*.

of the ligand are essential for the receptor-ligand molecular interactions. The guanidine group of Arg in the ligand forms hydrogen bonds with the β-carboxylic atoms of D150 and D218 in the α_V subunit, whereas the β-carboxylic group of Asp in the ligand participates in hydrogen bonding with the NH groups in the backbones of N215 and Y122 in the β_3 subunit. In addition, the β-carboxyl group of Asp participates in coordination of divalent Ca^{2+} ion (32). The latter interaction is very important because the entire process of ligand binding and activation of integrins is cation-dependent (3).

Consequently, we explored the possibility of simplifying the bioactive motif by using RD (arginine-aspartic acid) containing hexapeptides in our molecular design. Unlike large biomolecular carriers such as antibodies, the use of small peptide derivatives for molecular imaging are advantageous because they diffuse rapidly into tumors and reduce the risk of inducing immunologic reactions *in vivo*. Additionally, small bioactive molecules are amenable to combinatorial and parallel syntheses for optimizing their biological activities. Generally, small molecules allow large-scale synthesis, high-quality control of the products, and enhanced data reproducibility.

Our synthetic procedure involved the preparation of Cypate, peptide, and Cypate–peptide conjugates. Recently, we described an improved method for the synthesis of Cypate, a biocompatible NIR fluorescent dye (24). Cypate was conjugated to peptides prepared on solid support by standard Fmoc peptide synthesis strategy, as reported (26). The final product was purified by HPLC and characterized by LC-MS and spectrophotometric methods. For comparison, we also prepared and evaluated analogous linear (Cypate-GRGDSPK-OH, Cyp-RGD) and cyclic (cyclo[RGDfVK(ε-Cypate)], Cyp-cyclo-RGD) peptides. The new GRD peptide differs from the linear RGD peptide known to bind ABI (22) in that it lacks the glycine between the arginine and the aspartic acid of the RGD peptide. This cyclic peptide is known to bind strongly to ABI (33). Unlike cyclic RGD peptides, the linear GRD peptide does not require additional cyclization steps to obtain the peptide in good yields and high purity (>95% HPLC purity). To further study the tumor uptake of the GRD peptide by nuclear methods, we also prepared the DOTA-GRD conjugate by the standard procedure as reported (26). Radiolabeling the DOTA conjugates with radiometals such as ^{64}Cu and ^{111}In allows for their use in positron emission tomography (34) and gamma scintigraphy (35), respectively.

A549 Tumor Cells Express ABI. The human non-small cell carcinoma cell line, A549, is widely used to study the role of integrins in normal and pathophysiological processes (36–44). We validated the presence of ABI in this tumor model by Western blot and immunohistochemistry (IHC). Western blot analysis (see supporting information) shows bands corresponding to the two integrin (α and β) subunits of ABI from A549 tumor cell membrane. These bands were absent in the ABI-negative HeLa

cell membrane. Similarly, IHC on A549 cells demonstrated the presence of α_v and β_3 integrins, which appear as a brown stain (see supporting information). This staining is not seen in negative control slides, which were not treated with primary antibody. Interestingly, the β_3 subunit is expressed at a higher level in A549 than the α_v subunit. This finding suggests that β_3 may also be associated with another α subunit in the tumor cell. These observations justified our choice of the A549 cell line to study integrin-mediated retention of the molecular probes in tumors.

Cypate-GRD Molecular Probe Is Not Cytotoxic to A549 Cells. We used the MTT assay to determine the cytotoxicity of Cyp-GRD on A549 tumor cells. The conventional MTT protocol typically involves background subtraction at 690 nm from the absorbance at 570 nm. However, our data were not consistent with this procedure because of interference from the tail absorption of Cypate at 690 nm. This interference resulted in proportional increase in the background subtraction signal with increasing probe concentration, yielding false-positive cytotoxicity data. To circumvent this problem, we adjusted the background absorbance at 690 nm by running parallel experiments with and without MTT. The adjusted absorbance was obtained by subtracting the pre-MTT absorbance from the post-MTT value. We also observed that eliminating phenol red from the cell culture media gave reproducible results. The results showed that Cyp-GRD did not induce cell proliferation or cytotoxicity, up to 100 μM solution in 20% aqueous DMSO (see supporting information). This observation suggests that Cyp-GRD can be used as a purely diagnostic probe with no obvious deleterious effects on normal cell cycle and functions.

Cypate-GRD Probe Internalized by A549 Cells. To assess the uptake of Cyp-GRD in cells, we incubated 1 μM Cyp-GRD with A549 cells for 30 min at 4°C and 37°C. Fig. 1*a* shows that the Cyp-GRD conjugate was internalized by A549 cells at 37°C. The image shows a mature cell with well defined nucleus and a mitotic cell at the last stages of cell division with the probe uniformly partitioned between the two dividing cells. In contrast, the conjugate remained in the peripheral region of the cell membrane at 4°C (data not shown). These features are reminiscent of G protein-coupled receptor-mediated endocytosis of ligands (45, 46). Specific inhibition of Cyp-GRD binding to A549 cells with commercially available ABI-avid cyclic peptide, cyclo[Arg-Gly-Asp-D-Phe-Val] (Fig. 1*b*) and the inability of a non-ABI ligand, octreotate (47), to inhibit the internalization of Cyp-GRD in the cells further demonstrated that Cyp-GRD targets a common integrin as RGD peptides. To further assess the mechanism of internalization, we performed blocking studies with anti-α_v and anti-β_3 functionally tested mAbs (Molecular Probes) by coincubating A549 cells in a mixture of 10 μM mAb and 1 μM Cyp-GRD at 37°C. As shown in Fig. 1, internalization of Cyp-GRD was inhibited by anti-β_3 mAb (Fig. 1*c*) and to a lesser extent by anti-α_v (Fig. 1*d*). These data suggest that the β_3 integrin

Fig. 2. *In vivo* distribution of Cyp-GRD in mice. (*a*) White light image of A549 tumor-bearing mice. (*b* and *c*) Fluorescence image of Cypate-RGD peptide conjugate in A49 tumor-bearing mouse at 5 min (*b*) and at 24 h (*c*) after injection. (*d*) *Ex vivo* image of selected organ parts at 20 h after injection. (*e*) Inhibition of the binding of Cypate-Cyp-GRD by cyclo(RGDfV) at 24 h. All images are on the same relative fluorescence intensity scale (−9 to 400).

subunit plays a vital role in the binding of Cyp-GRD and probably initiates the receptor-specific internalization of the probe in A549 cells. The high expression of the β_3 relative to the α_v integrin subunit in A549 cells, as shown by both immunohistochemistry and Western blot analysis support the dominant role of β_3 integrin in the molecular recognition of Cyp-GRD. The fact that Cyp-GRD does not translocate to the nucleus further augments its value as a molecular imaging probe (Fig. 1*e*).

Cypate-GRD Is Selectively Retained by A549 Tumor. Optical projection imaging is a simple method to rapidly evaluate the distribution of fluorescent molecular probes in tumors *in vivo*. The instrument used consists of two nominal 780-nm collimated solid state laser diodes for excitation and a charge-coupled device camera (12 bit, 1024 × 1024 pixel, back illuminated) equipped with an interference filter to capture the emitted light at 830 nm. Injection of the Cyp-GRD probe (100 μl; 0.3 μmol/kg body weight) into A549 tumor-bearing nude mice (≈5-mm diameter tumors), and subsequent time-sequence optical imaging, showed preferential uptake of the probes in the tumor (Fig. 2) relative to normal tissues. The barely palpable tumor is located on the lower left flank of the mouse (Fig. 2*a*). The whole animal fluoresced up to 2 h after infection of the probe before the probe started to clear from blood and nontarget tissues (Fig. 2*b*). The selective uptake of the molecular probe in tumor became obvious after 8 h after infection when the probe significantly cleared from nontarget tissues. By 24 h after infection, the tumor was clearly visible (Fig. 2*c*). The observed slow clearance of Cyp-GRD from blood would favor multiple internalization of the circulating probe in the ABI-positive tumor because this receptor can translocate from the cytoplasm back to the cell surface after internalizing the ligand. This rebound effect is similar to the internalization mechanism observed in other G protein-coupled receptors and has the positive effect of concentrating the receptor-specific probes and drugs in target cells (45, 46). *Ex vivo* analysis of the normalized fluorescence intensity (relative to blood) clearly shows a high intensity of the fluorescence emission from the tumor tissue (Fig. 2*d*). This corroborated the noninvasive *in vivo* imaging of the probe distribution and showed that Cyp-GRD selectively accumulated in the tumor tissue and major excretion organs.

We also evaluated the distribution of Cyp-RGD and Cyp-

cyclo-RGD in A549 *in vivo* (Fig. 3*a*). Expectedly, retention of the cyclic RGD peptide conjugate in the tumor was higher by a factor of three compared with the linear RGD analogue but its accumulation in nontarget tissues was equally high. The linear RGD peptide conjugate was primarily retained in the liver and the kidneys. Surprisingly, the tumor uptake of these conventional

Fig. 3. *Ex vivo* profile of molecular probe distribution. (*a*) Distribution of the Cyp-GRD, Cyp-RGD, and Cyp-cyclo-RGD in the selected organ parts of A549 tumor-bearing mice. The fluorescence intensity is relative to blood (n = 3) and normalized to the organ with highest intensity. (*b*) Distribution of Cyp-RGD with (black bars) and without (white bars) cyclic RGD peptide inhibitor, cyclo[RGDfV].

Fig. 4. Spatial distribution of Cyp-GRD in tumor tissue. (*a*) *Ex vivo* stacked fluorescence images of Cyp-GRD distribution in A549 tumor tissue at different depths. (*b*) Three-dimensional fluorescence image of Cyp-GRD in ex-vivo A549 tumor tissue 24 h after injection of Cyp-RGD. (*c*) Correlation between mitochondrial NADH expression level and Cyp-GRD distribution in A549 tumor 24 h after injection (900-μm scan surface).

RGD probes was low, compared with Cyp-GRD at 24 h after infection. Apart from the liver and kidneys, Cyp-GRD uptake in nontarget organs was minimal. Therefore, deletion of glycine from the RGD peptide sequence favored its binding to ABI, presumably through initial binding to the β_3 integrin subunit.

We further tested the hypothesis that the GRD peptide was solely responsible for the tumor uptake by injecting ^{111}In-DOTA-GRD (120 μCi; 1 Ci = 37 GBq) into A549 tumor-bearing mice. Time-sequence scintigraphy showed a rapid renal clearance of the probe, with nearly all of the material localized in the bladder at 30 min after infection. Furthermore, the precursor dye Cypate was not retained in the tumor, but was rapidly cleared from blood by the liver within 4 h after infection. This is also in agreement with the *in vitro* data that showed that Cypate did not internalize in A54 cells. These intriguing observations demonstrate the significantly synergistic effects of the dye and peptide to enhance the retention of Cyp-GRD in A549 cells and tumor tissue.

To evaluate the extent of nonspecific uptake, we injected the nonspecific agent ICG and a non-ABI-avid Cypate-octapeptide conjugate (cytate) (21) into different A549 tumor-bearing mice. These non-ABI-specific probes were not retained in the A549 tumor tissue, but predominantly accumulated in the liver within 1 h after infection of the probes. This distribution is similar to the hepatobiliary excretion pathway observed in normal rats (21) and in humans using ICG (48).

To further demonstrate the specificity of the Cyp-GRD, we used cyclo(RGDfV), which has high specificity and affinity for ABI (33), to competitively inhibit the uptake of the optical probe. Coinjection of equimolar concentrations (0.3 μmol/kg body weight) of Cyp-GRD and cyclo(RGDfV) significantly blocked Cyp-GRD uptake in the tumor at 24 h after infection (Figs. 2*e* and 3*b*). The inhibition of Cyp-GRD uptake by cyclo(RGDfV) shows that the both compounds bind to the same receptor protein or that the binding of cyclo(RGDfV) inhibits the uptake of Cyp-GRD by an allosteric effect.

These results clearly demonstrate the synergistic effects of the molecular probe and GRD peptide for ABI molecular recognition. The findings suggest the potential of using carbocyanine probes as optical scaffolds for designing biologically active molecules.

Distribution of Cypate-GRD in A539 Tumor Tissue Is Heterogenous and Correlates with Mitochondrial NADH. The noninvasive optical imaging by reflectance method images the probe distribution within a depth of a few millimeters from tissue surface. The isotropic fluorescence emission captured by the charge-coupled device camera appears to indicate uniform distribution of the probe in tumor tissue. However, the heterogeneity of tumor cells

suggests that ABI and other protein receptors are not uniformly distributed within the tumor tissue. To explore this possibility, we used the snap-freeze method described by Gu *et al.* (27), which preserves tissue and its redox state for subsequent characterization by high-resolution *ex vivo* fluorescence imaging. The method is akin to *in situ* histologic staining, except that fluorescence from the probe retained by the tumor and other endogenous fluorophores is used to characterize the tissue. The tumor was excised from the animal and imaged at 100-μm depth intervals by removing the appropriate layer of tissue for each step. Fig. 4*a* shows the stacked image of the tumor and demonstrates the heterogeneity of the probe distribution at different tumor depths in the *Z* direction. The tumor cells were typically mixed with normal (stromal) cells that have low uptake of the probe (blue to green regions in Fig. 4*a*). Although the heterogeneous nature of tumors allows them to evade treatment, targeting these abnormal cells with integrin-specific drugs can selectively destroy the tumor cells while preserving healthy tissues.

As described (27), the snap-freeze method also provides information about the metabolic state of the cells through measurement of mitochondrial NADH and FP levels. The ratio of these biomolecules in mitochondria is an index of cellular metabolic activity. The large differences in the excitation (365, 440, and 780 nm) and emission (455, 520, and 830 nm) wavelengths of NADH, FP, and Cyp-GRD, respectively, minimize spectral overlap; this facilitates imaging the distribution of all three molecules in the same tissue and correlating their relative expression levels with the metabolic state of the tumor. Fig. 4*b* shows the heterogenous 3D fluorescence image of Cyp-GRD at 900 μm from the scan surface. A remarkable spatial correlation between the reduced state (high NADH) and Cyp-GRD distribution was observed at different tumor depths (Fig. 4*c*). In contrast, oxidized FP expression (oxidized state), and the overall oxidized [FP/(FP + NADH)] and reduced [NADH/(FP + NADH)] state ratios of the tumor are less spatially correlated to Cyp-GRD distribution. The reason for the strong correlation with NADH but not with FP or redox ratios is not clear at this time. A possible mechanism could involve NAD-mediated oxidation of the polymethine chain of Cypate *in vivo* and the subsequent conversion of the nonfluorescent NAD to NADH. This process would result in the correlation of the local Cyp-GRD distribution with NADH but not the global redox state of the tumor.

Conclusion

We have designed and prepared a novel NIR molecular probe that is selectively retained by ABI-positive tumors *in vitro* and *in vivo*. *In vivo* studies showed that this peptide conjugate accu-

mulated at higher levels compared with the Cypate conjugates of conventional linear and cyclic peptides. Blocking studies with a known ABI-avid cyclic RGD peptide inhibited the binding of Cypate-GRD, suggesting that both compounds target the same active site of the protein. Additional studies with Cypate conjugates of conventional RGD peptides showed low retention in A549 tumor. These findings attest to the synergistic effects of both the optical antenna and the GRD peptide in ABI molecular recognition. The data demonstrate that the structural framework of carbocyanine dyes can act as fluorescent antennae and optical scaffolds for discovering new bioactive entities and optimizing the bioactivity of small biomolecules for a target protein receptor. Interestingly, *ex vivo* redox studies show that the level of probe accumulation in ABI-positive tumors, which relates to integrin expression, correlates with mitochondrial NADH concentration. Thus, uptake of the Cypate-GRD in tumor cells may indicate the local metabolic status (reduced sate) of the cells or tissue.

1. Carmeliet, P. & Jain, R. K. (2000) *Nature* **407,** 249–257.
2. Arnaout, M. A. (2002) *Immunol. Rev.* **186,** 125–140.
3. Arnaout, M. A., Goodman, S. L. & Xiong, J. P. (2002) *Curr. Opin. Cell Biol.* **14,** 641–651.
4. Humphries, M. J. (2002) *Arthritis Res.* **4,** Suppl. 3, S69–S78.
5. Manes, T., Zheng, D.-Q., Tognin, S., Woodard, A. S., Marchisio, P. C. & Languino, L. R. (2003) *J. Cell. Biol.* **161,** 817–826.
6. Sakakura, C., Hagiwara, A., Nakanishi, M., Shimomura, K., Takagi, T., Yasuoka, R., Fujita, Y., Abe, T., Ichikawa, Y., Takahashi, S., *et al.* (2002) *Br. J. Cancer* **87,** 1153–1161.
7. Ellegala, D. B., Poi, H. L., Carpenter, J. E., Klibanov, A. L., Kaul, S., Shaffrey, M. E., Sklenar, J. & Lindner, J. R. (2003) *Circulation* **108,** 336–341.
8. Haubner, R., Wester, H. J., Weber, W. A., Mang, C., Ziegler, S. I., Goodman, S. L., Senekowitsch-Schmidtke, R., Kessler, H. & Schwaiger, M. (2001) *Cancer Res.* **61,** 1781–1785.
9. Sipkins, D. A., Cheresh, D. A., Kazemi, M. R., Nevin, L. M., Bednarski, M. D. & Li, K. C. P. (1998) *Nat. Med.* **4,** 623–626.
10. Plow, E. F., Haas, T. K., Zhang, L., Loftus, J. & Smith, J. W. (2000) *J. Biol. Chem.* **275,** 21785–21788.
11. Edwards, W. B., Anderson, C. J., Fields, G. B. & Welch, M. J. (2001) *Bioconjugate Chem.* **12,** 1057–1065.
12. Harris, T. D., Kalogeropoulos, S., Nguyen, T., Liu, S., Bartis, J., Ellars, C., Edwards, S., Onthank, D., Silva, P., Yalamanchili, P., *et al.* (2003) *Cancer Biother. Radiopharm.* **18,** 627–641.
13. van Hagen, P. M., Breeman, W. A. P., Bernard, H. F., Schaar, M., Mooij, C. M., Srinivasan, A., Schmidt, M. A., Krenning, E. P. & de Jong, M. (2000) *Int. J. Cancer* **90,** 186–198.
14. Rintoul, R. C. & Sethi, T. (2002) *Clin. Sci.* **102,** 417–424.
15. Schraa, A. J., Kok, R. J., Moorlag, H. E., Bos, E. J., Proost, J. H., Meijer, D. K. F., de Leu, L. & Molema, G. (2002) *Int. J. Cancer* **102,** 469–475.
16. Schiffelers, R. M., Molema, G., ten Hagen, T. L. M., Janssen, A., Schraa, A. J., Kok, R. J., Koning, G. A. & Storm, G. (2002) *J. Liposome Res.* **12,** 129–135.
17. Janssen, M. L., Oyen, W. J., Dijkgraaf, I., Massuger, L. F., Frielink, C., Edwards, D. S., Rajopadhye, M., Boonstra, H., Corstens, F. H. & Boerman, O. C. (2002) *Cancer Res.* **62,** 6146–6151.
18. Hawrysz, D. J. & Sevick-Muraca, E. M. (2000) *Neoplasia* **2,** 388–417.
19. Ntziachristos, V., Ripoll, J. & Weissleder, R. (2002) *Opt. Lett.* **27,** 333–335.
20. Achilefu, S. (2004) *Technol. Cancer Res. Treat.* **3,** 393–409.
21. Achilefu, S., Dorshow, R. B., Bugaj, J. E. & Rajagopalan, R. (2000) *Invest. Radiol.* **35,** 479–485.
22. Dechantsreiter, M. A., Planker, E., Matha, B., Lohof, E., Holzemann, G., Jonczyk, A., Goodman, S. L. & Kessler, H. (1999) *J. Med. Chem.* **42,** 3033–3040.
23. Achilefu, S., Jimenez, H. N., Dorshow, R. B., Bugaj, J. E., Webb, E. G., Wilhelm, R. R., Rajagopalan, R., Johler, J. & Erion, J. L. (2002) *J. Med. Chem.* **45,** 2003–2015.
24. Ye, Y. P., Bloch, S. & Achilefu, S. (2004) *J. Am. Chem. Soc.* **126,** 7740–7741.
25. Atherton, E. & Sheppard, R. C. (1989) *Solid Phase Peptide Synthesis: A Practical Approach* (Oxford Univ. Press, Oxford).
26. Achilefu, S., Wilhelm, R. R., Jimenez, H. N., Schmidt, M. A. & Srinivasan, A. (2000) *J. Org. Chem.* **65,** 1562–1565.
27. Gu, Y. Q., Qian, Z. Y., Chen, J. X., Blessington, D., Ramanujam, N. & Chance, B. (2002) *Rev. Sci. Instrum.* **73,** 172–178.
28. Haubner, R. & Wester, H. R. (2004) *Curr. Pharm. Design* **10,** 1439–1455.
29. Bloch, S., Liang, K., Dorshow, R. B., Ye, Y. & Achilefu, S. (2004) *Proc. SPIE* **5329,** 222–228.
30. Chen, X., Shahinian, A. H., Park, R., Bozorgzadeh, M. H., Bading, J. R. & Conti, P. S. (2003) *J. Nucl. Med.* **44,** 47P–48P.
31. Xiong, J. P., Stehle, T., Diefenbach, B., Zhang, R., Dunker, R., Scott, D. L., Joachimiak, A., Goodman, S. L. & Arnaout, M. A. (2001) *Science* **294,** 339–345.
32. Xiong, J. P., Stehle, T., Zhang, R., Joachimiak, A., Frech, M., Goodman, S. L. & Arnaout, M. A. (2002) *Science* **296,** 151–155.
33. Haubner, R., Wester, H. J., Burkhart, F., Senekowitsch-Schmidtke, R., Weber, W., Goodman, S. L., Kessler, H. & Schwaiger, M. (2001) *J. Nucl. Med.* **42,** 326–336.
34. Anderson, C. J., Dehdashti, F., Cutler, P. D., Schwarz, S. W., Laforest, R., Bass, L. A., Lewis, J. S. & McCarthy, D. W. (2001) *J. Nucl. Med.* **42,** 213–221.
35. Breeman, W. A. P., de Jong, M., Erion, J. L., Bugaj, J. E., Srinivasan, A., Bernard, B. F., Kwekkeboom, D. J., Visser, T. J. & Krenning, E. P. (2002) *J. Nucl. Med.* **43,** 1650–1656.
36. Cordes, N., Beinke, C., Plasswilm, L. & van Beuningen, D. (2004) *Strahlenther. Onkol.* **180,** 157–164.
37. Oyama, T., Sykes, K. F., Samli, K. N., Minna, J. D., Johnston, S. A. & Brown, K. C. (2003) *Cancer Lett.* **202,** 219–230.
38. Lubin, F. D., Segal, M. & McGee, D. W. (2003) *Immunology* **108,** 204–210.
39. Davison, E., Kirby, I., Whitehouse, J., Hart, I., Marshall, J. F. & Santis, G. (2001) *J. Gene. Med.* **3,** 550–559.
40. Triantafilou, K., Triantafilou, M., Takada, Y. & Fernandez, N. (2000) *J. Virol.* **74,** 5856–5862.
41. Allen, C. M., Sharman, W. M., La Madeleine, C., Weber, J. M., Langlois, R., Ouellet, R. & van Lier, J. E. (1999) *Photochem. Photobiol.* **70,** 512–523.
42. Pottratz, S. T. & Weir, A. L. (1997) *Eur. J. Clin. Invest.* **27,** 17–22.
43. Reilly, P. L., Woska, J. R., Jeanfavre, D. D., McNally, E., Rothlein, R. & Bormann, B. J. (1995) *J. Immunol.* **155,** 529–532.
44. Bai, M., Campisi, L. & Freimuth, P. (1994) *J. Virol.* **68,** 5925–5932.
45. Whetstone, P. A., Akizawa, H. & Meares, C. F. (2004) *Bioconjugate Chem.* **15,** 647–657.
46. Gao, B. C., Curtis, T. M., Blumenstock, F. A., Minnear, F. L. & Saba, T. M. (2000) *J. Cell Sci.* **113,** 247–257.
47. Balon, H. R., Goldsmith, S. J., Siegel, B. A., Silberstein, E. B., Krenning, E. P., Lang, O. & Donohoe, K. J. (2001) *J. Nucl. Med.* **42,** 1134–1138.
48. Engelking, L. R., Anwer, M. S. & Lofstedt, J. (1985) *Am. J. Vet. Res.* **46,** 2278–2284.

MEDICAL SCIENCES